8 Urologic Neoplasms: Prostate, Bladder, and Renal Cell Carcinoma

Bhushan Desai and Hossein Jadvar

Prostate Cancer

Case 8.1

History

A 60-year-old Caucasian male with castrate-resistant metastatic adenocarcinoma of prostate, status post radical prostatectomy (Gleason score 4 + 5) and androgen ablation therapy.

Findings

FDG PET-CT scan performed 4 months after the baseline showed an interval increase in extent and degree of hypermetabolism diffusely throughout both hepatic lobes with maximum SUV of 9.1 (Fig. 8.1). There is also an interval increase in number and size of diffuse pulmonary nodules. Patient died from disseminated disease 2 months later.

Impression

Interval progression of metastatic disease.

Case 8.2

History

A 55-year-old male with history of end-stage renal disease and metastatic prostate cancer, initially diagnosed in June 2005, status post radiation treatment and currently on Casodex and monthly Lupron.

P.S. Conti, A. Kaushik (eds.), *PET-CT*, DOI 10.1007/978-1-4419-5811-2_8

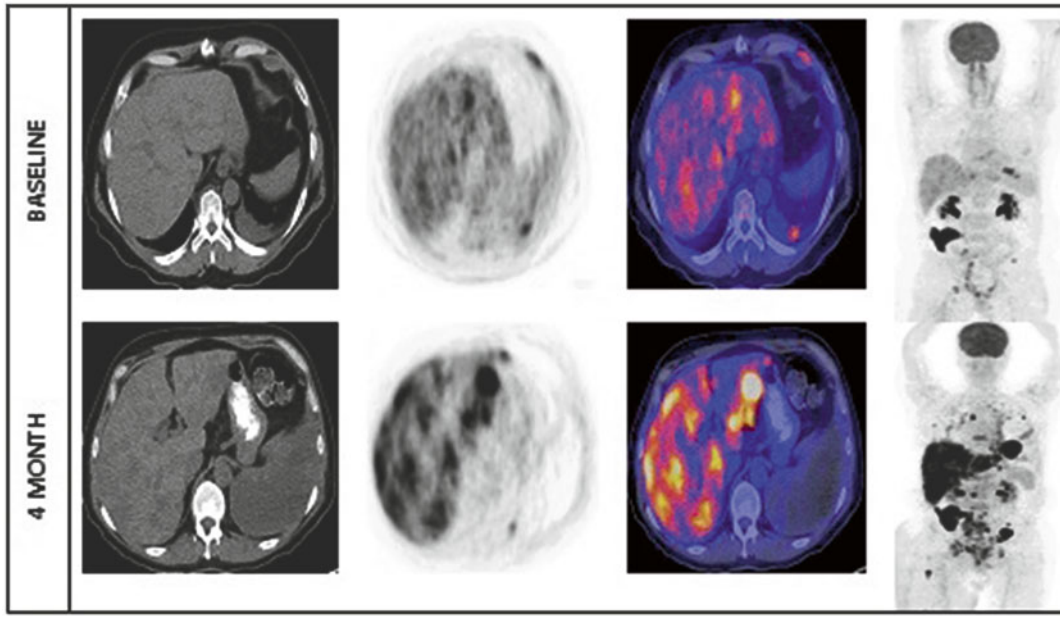

Fig. 8.1

Findings

There has been an interval increase in the size and metabolic activity of previously seen mesenteric, retroperitoneal, and right common iliac lymph nodes (Fig. 8.2). For example, the hypermetabolic left para-aortic lymph nodes, at L2 level, now have a maximum SUV of 2.7 (from 2.1). A newly apparent, hypermetabolic left supraclavicular lymph node has a SUVmax of 3.0 and measures 1.5 cm × 2.9 cm. There has also been an interval increase in the intensity and extent of previously seen hypermetabolic osseous lesions.

Impression

Progressive retroperitoneal, left supraclavicular lymphadenopathy, and osseous metastatic disease.

Case 8.3

History

A 63-year-old male with castrate-resistant metastatic prostate cancer (primary Gleason score 4 + 5).

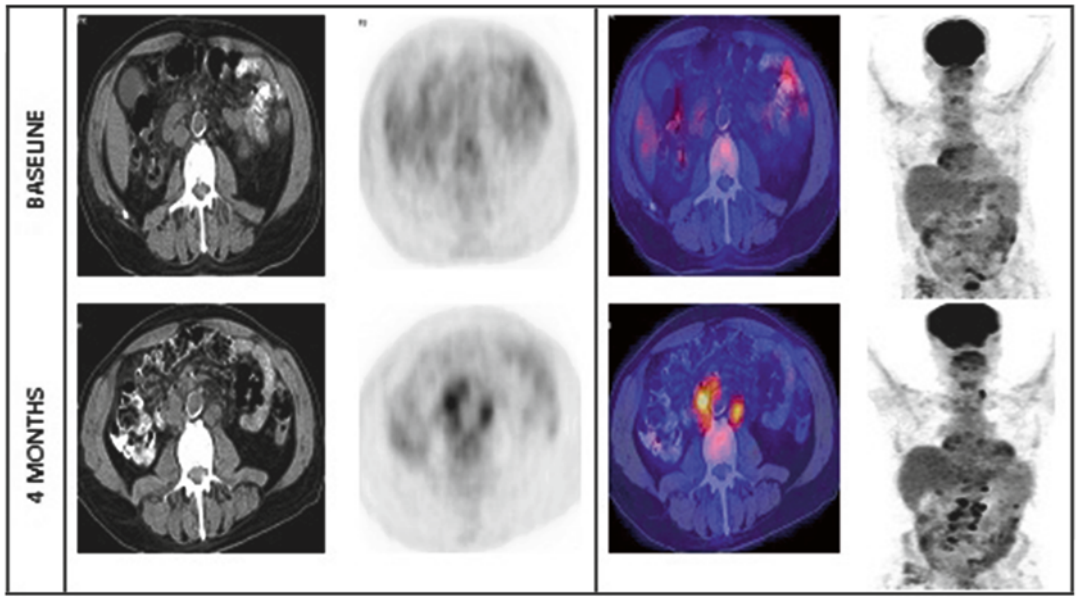

Fig. 8.2

Findings

Serial FDG PET-CT scans showed that the lesions' metabolic activity, as depicted by SUVmax, kept on decreasing showing a good response to therapy and was also correlated with decline in PSA values, but the CT density, as depicted by HU (Hounsfield unit), continued to increase (Fig. 8.3).

Impression

Metabolic activity of metastatic osseous lesions tends to decrease, while CT density tends to increase with successful therapy.

Case 8.4

History

An 86-year-old male, recently diagnosed with small cell carcinoma of the prostate gland. PET-CT is done as part of the initial treatment strategy evaluation.

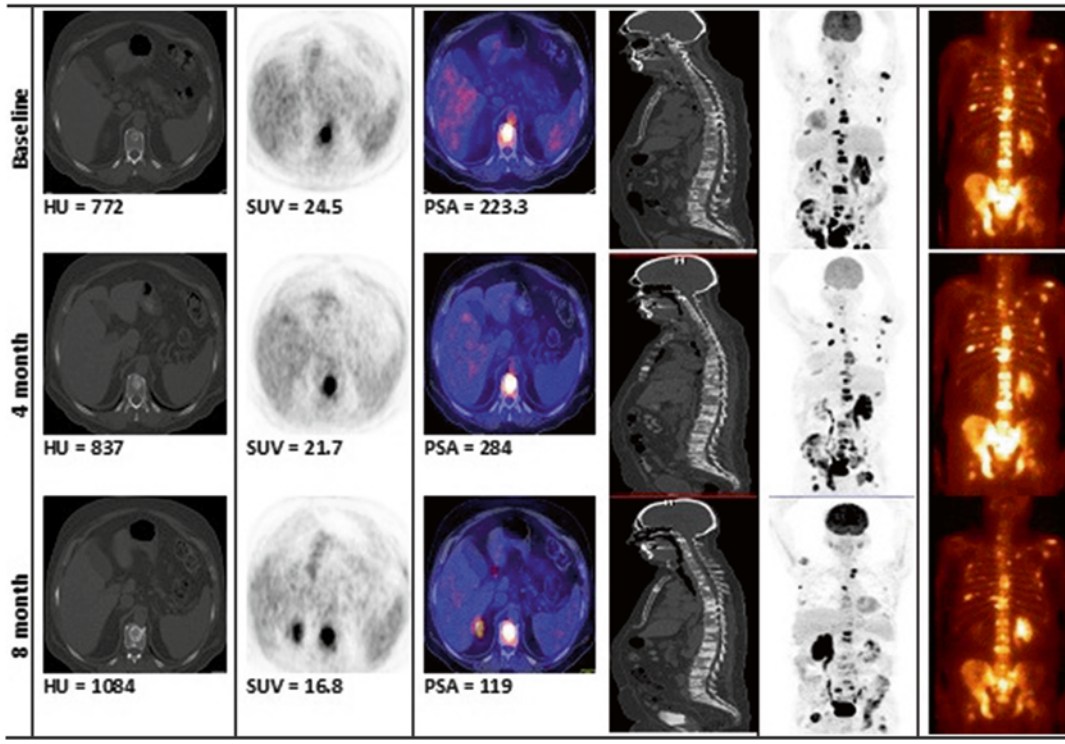

Fig. 8.3

Findings

The prostate gland is extensively bulky with areas of calcification (Fig. 8.4). Intense metabolic activity is seen at the right posterior and central aspect of prostate (SUVmax 11.2), compatible with known primary neoplasm. The prostate tumor appears to encroach the urethra with no fat plane identified between the prostate tumor and anterior wall of the rectum posteriorly or the urinary bladder anteriorly. There are several hypermetabolic bilateral external and internal iliac and presacral/perirectal lymph nodes, compatible with metastatic disease. The highest level of FDG-avid lymph node is seen at the level of left proximal external iliac bifurcation, involving the left external iliac lymph node, measuring approximately 2.7 cm in long axis with SUVmax 13.3. The largest hypermetabolic right external iliac lymph node measures approximately 2.6 cm long axis with SUVmax 14.6. Two hypermetabolic presacral lymph nodes are seen: one in the midline shows SUVmax 7.0, and the left paramedian presacral lymph node shows SUVmax 9.4. A right perirectal lymph node at the level of S4 shows SUVmax 13.1.

Impression

Hypermetabolic, large, bulky tumor involving right and central posterior aspect of prostate with hypermetabolic, metastatic bilateral internal and external iliac and perirectal/presacral lymphadenopathy.

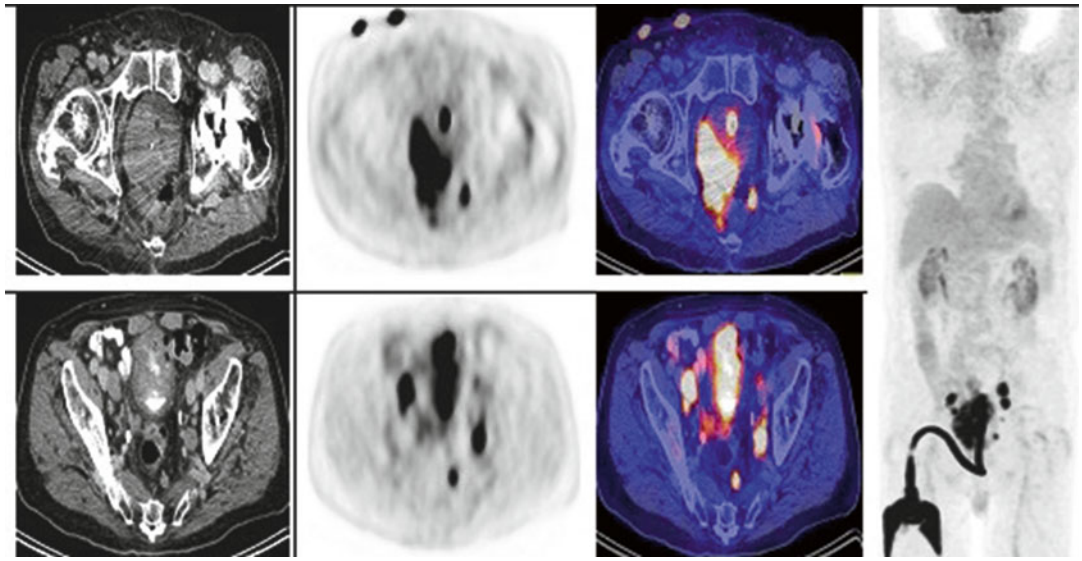

Fig. 8.4

Pearls and Pitfalls

- FDG PET may be useful for detecting, staging, and restaging poorly differentiated, hypoxic, high Gleason score tumors, monitoring treatment response in metastatic disease, assessment of extent of metabolically active castrate-resistant disease, and prognostication.
- FDG PET-CT has limited utility to differentiate between primary prostate cancer vs. BPH and post-op scarring and in patients with local recurrence after primary therapy.
- Higher FDG uptake with higher Gleason grade, advanced clinical stage, and higher serum PSA levels.
- Conventional morphologic (CT) and functional (99m Tc-MDP bone scintigraphy) imaging methods for qualitative treatment response assessment of bone metastases have been inaccurate and pose a challenge in routine oncological practice and in clinical trials, as skeletal lesions have been considered as nonmeasurable disease [2].
- Semiquantitative analysis of 18F FDG PET-CT might address an urgent need to develop an objective method for assessing tumor response in bone lesions which can clinically help physicians determine the effectiveness of systemic therapy [11, 13].

Discussion

Prostate cancer is the most common CA (30 % of all male CA) and second leading cause of CA death in men (exceeded by lung cancer) [1]. Incidence of adenocarcinoma is much higher than sarcoma and transitional cell carcinoma of the prostate. Routine diagnostic tests include digital rectal examination (DRE), PAP and PSA (nonspecific), and Gleason score (min 2, max 10). PSA and DRE have a limited positive predictive

value. Imaging modalities currently in use are ultrasonography (standard gray scale, enhanced transrectal with contrast agents, color and power Doppler, elastrography), computed tomography (CT), MRI (endorectal probe, contrast, spectroscopic imaging, lymphotropic nanoparticles, DWI), scintigraphy (bone scan, radioimmunoscintigraphy—*Prostascint*™), and positron emission tomography (PET), PET-CT, and PET-MRI.

Prostate cancer is biologically and clinically a heterogeneous disease, and its imaging evaluation needs to be tailored to the specific phases of the disease in a patient-specific, risk-adapted manner. Within 10 years after successful treatment for localized disease, 15–40 % experience PSA rise which is termed as biochemical recurrence. About 25–35 % of men with an increasing serum PSA level will develop locally recurrent disease only, 20–25 % will develop metastatic disease only, and 45–55 % will develop both local recurrence and metastatic disease. Median survival time for patients detected with metastatic disease is around 5 years, while the medial survival is only 8–18 months for those who have become refractory to hormonal therapy. As shown in Case 1, the patient had developed castrate-resistant metastatic prostate cancer and died 2 months after his 4-month scan due to disease progression.

Bone is the most common site to which prostate cancer metastasizes. Response to treatment is typically estimated by using a combination of methods, including diagnostic imaging, measurement of biochemical markers, and evaluation of patients' symptoms. Three patterns of bone metastasis commonly noted depending on the stage of treatment are (a) FDG uptake without corresponding morphological changes on CT; (b) FDG uptake with concomitant morphological changes on CT as sclerotic, lytic, and/or mixed lesions; and (c) negative FDG PET but dense sclerosis on CT. Metabolic and anatomic details provided by the combined PET-CT may provide a good imaging tool for quantitatively assessing response of metastatic skeletal lesions to various forms of systemic therapy.

Several novel PET tracers which are being tested for use in prostate cancer are radiolabeled acetate (11C, 18F), choline (11C, 18F), 11C-methionine, dihydrotestosterone (18F-FDHT), anti-1-amino-3-18F--fluorocyclobutane-1-carboxylic acid (anti-18F-FACBC), 1-(2′-deoxy-2′-fluoro-b-D-arabinofuranosyl)thymidine (18F-FMAU), and [18F]DCFBC (PSMA inhibitor) [12, 14, 15].

Bladder Cancer

Case 8.5

History

A 68-year-old male with high-grade urothelial carcinoma primary involving his kidney and bladder with metastasis in the retroperitoneum and liver, status post open nephroureterectomy with excision of the bladder cuff and left pelvic lymph node dissection and chemotherapy. Scan is being done for restaging.

Findings

Interval progression of hepatic disease now pan lobar with interval increase in extent of right hepatic confluent metastatic disease with new active left hepatic lobe lesions (Fig. 8.5). The confluent disease in the right correlates to low attenuation and now measures 9.8 × 9.2 × 10.4 cm, with SUVmax 25.1 (9 × 6.6 × 4.1 cm with SUVmax 23.1 in prior). There is an interval increase in size and activity of portacaval nodes now with SUVmax 14.1 (right 13.5 in prior). Also noted is a new hypermetabolic gastroduodenal (SUVmax 16) celiac axis node which is normal sized. There are also new multiple retroperitoneal hypermetabolic nodes, for example, aortocaval nodes with SUVmax up to 8.9. Interval increase is seen in the extent of left anterior pillar of acetabulum medullary sclerosis with stable metabolic activity, now involving superior pubic ramus, with SUVmax 10.6 (SUVmax 9.8 in prior).

Impression

Interval progression of disease with increasing hepatic, nodal, and osseous metastases.

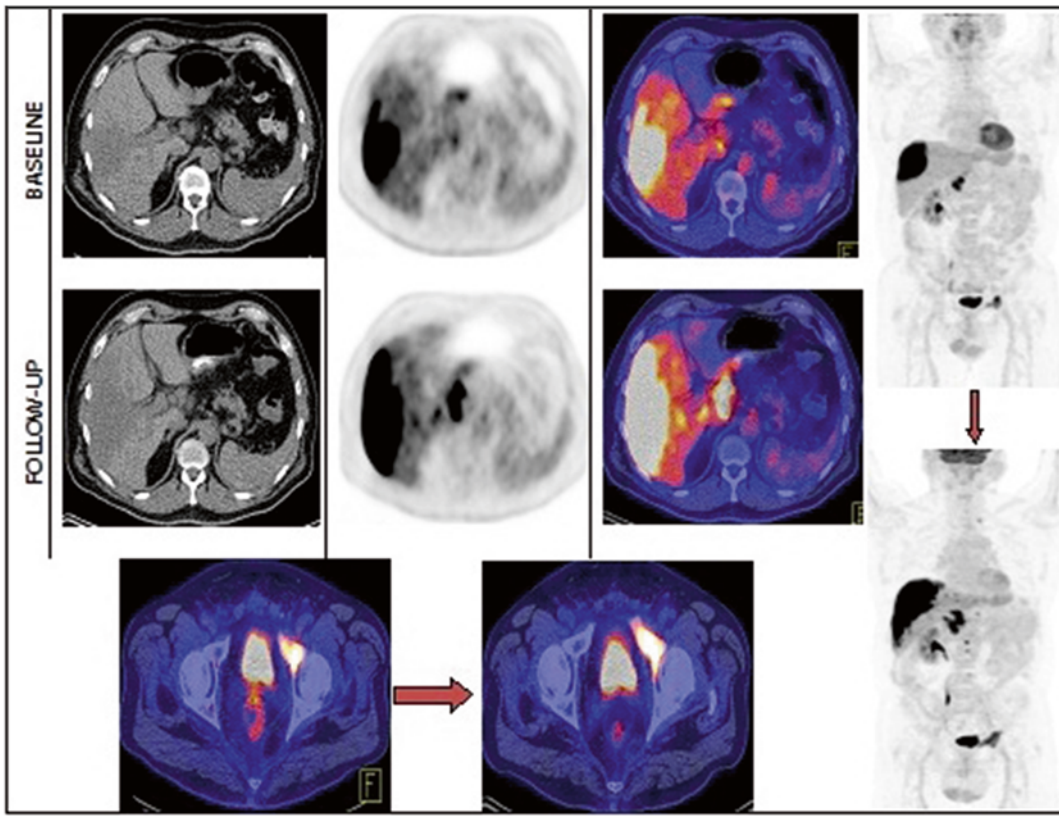

Fig. 8.5

Case 8.6

History

A 50-year-old male with history of metastatic bladder cancer, status post cystoprostatectomy with extensive lymph node dissection and seminal vasectomy with neobladder and ureteral diversion. The PET-CT was done for restaging purposes.

Findings

There is a slight misregistration of hypermetabolic activity with SUVmax 10.0 that most likely corresponds to the left supraclavicular lymph node, measuring approximately 0.6 × 0.8 cm (Fig. 8.6). There is large portacaval single lymph node or nodal conglomerate, approximately measuring 5.1 cm × 3.2 cm and demonstrating intense hypermetabolic activity (SUVmax 14.3). Patient is status post cystoprostatectomy with extensive lymph node dissection and seminal vasectomy with neobladder and ureteral diversion. The bilateral ureters are connected to the ileal conduit to Studer pouch and to urethra. There is stasis and dilatation of the left ureter and normal caliber of the right ureter, suggestive of stenosis at the anastomosis from left ureter to the conduit.

Impression

Scattered hypermetabolic lymph nodes above and below the diaphragm, with most active and largest lymph node/nodal conglomerate at portacaval location, consistent with metastatic disease.

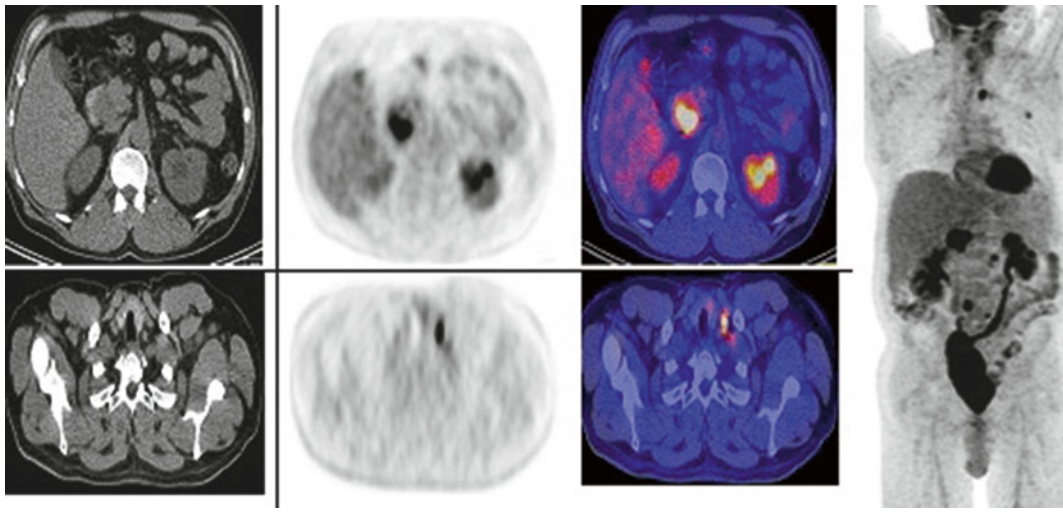

Fig. 8.6

Case 8.7

History

A 27-year-old male with bladder cancer, status post radical cystectomy and chemotherapy, with scan requested for initial staging.

Findings

There are several hypermetabolic periaortic and retroperitoneal lymph nodes noted; most of them are along the surgical clips (Fig. 8.7). The largest and the most active left aortic lymph node at the level of L4 vertebral body measures 1.3 cm with maximum SUV of 18.4. The left peritoneal nodule adjacent to the left psoas muscle measures 1.4 cm with maximum SUV of 8.6. The largest of right retroperitoneal lesion adjacent to the right psoas medially at the level of L5 vertebral body measures 2.9 cm × 2.4 cm with maximum SUV of 11.6. There are multiple presacral lesions with the largest presacral lesion next to the surgical clips on the left measures 3.1 cm × 2.5 cm with maximum SUV of 16. The midline presacral lesion measures 1.6 cm × 1.2 cm with maximum SUV of 10.7.

Impression

Multiple hypermetabolic abdominal and pelvic lymphadenopathy consistent with recurrent disease in the retroperitoneum.

Case 8.8

History

A 52-year-old female with recurrent high-grade urothelial carcinoma of the urinary bladder, status post radical cystectomy and anterior pelvic exenteration with multiple postoperative complications necessitating

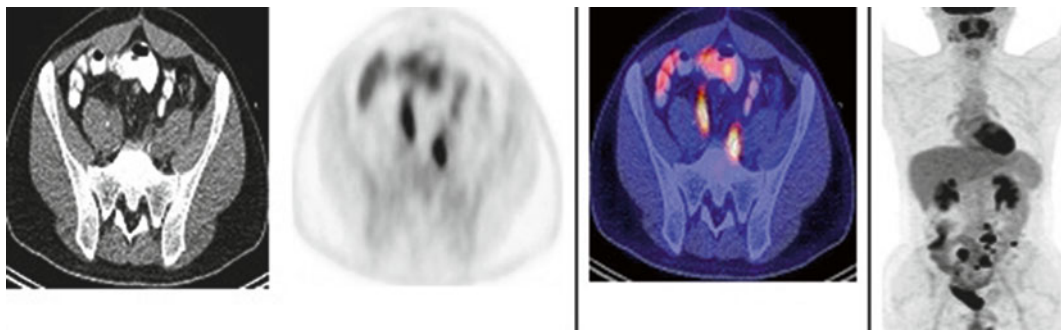

Fig. 8.7

additional six repair surgeries. Her last surgery included cystectomy with removal of the neobladder and ileal conduit urinary diversion and placement of bilateral open indwelling ureteral stents and biopsy of vaginal cuff. CABG pathology of the vaginal cuff revealed recurrent high-grade urothelial carcinoma. PET-CT is done to assess for local versus distant metastasis in order to plan further treatment strategy.

Findings

Left and right hydronephrosis and hydroureter are present (Fig. 8.8). Both ureters show mild circumferential wall thickening and terminate at the level of the large soft tissue mass at the L5–S1 level, suspicious for tumor involvement. There is hypermetabolic heterogeneous presacral mass, anterior to L5–S1, now measuring approximately $5.5 \times 5.3 \times 4.8$ with SUVmax 19.0. This tumor mass causes new bony erosion of approximately the anterior two-thirds of the upper sacrum. A focal intramuscular activity is noted laterally to the right ischial tuberosity, measuring approximately 1.0 cm and SUVmax 3.6, which may represent local inflammation versus metastatic implant.

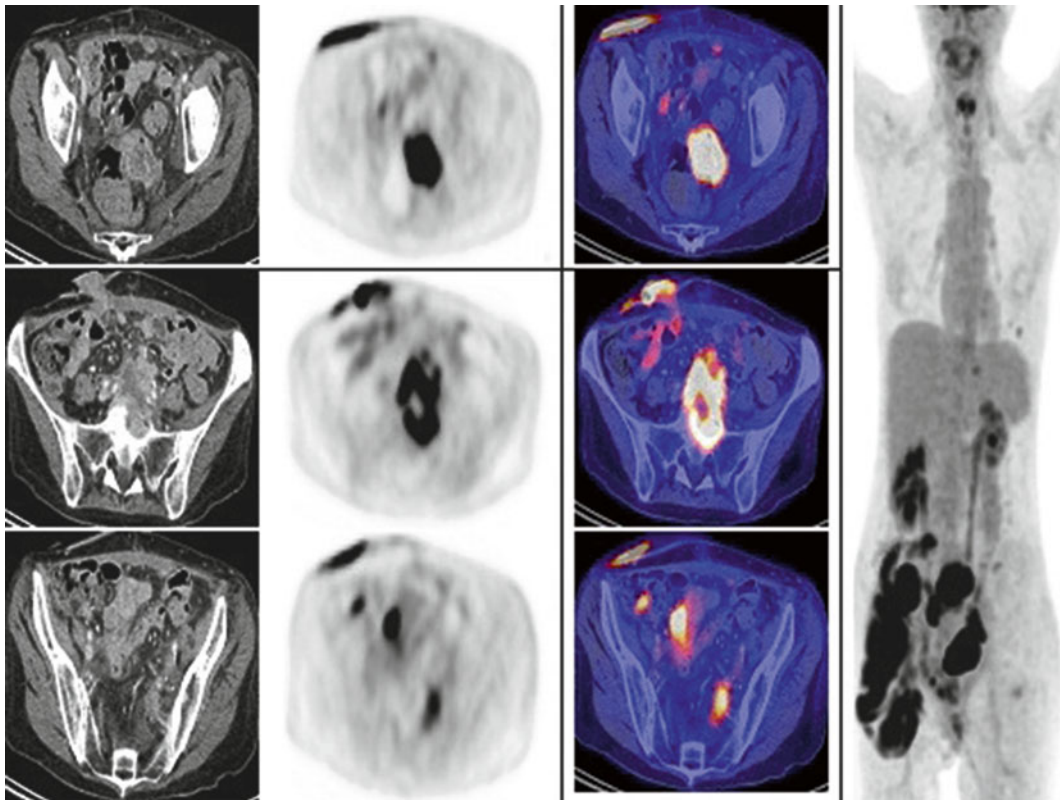

Fig. 8.8

Impression

Hypermetabolic lesions in the pelvis, significant in the presacral lesion which demonstrates bone erosion involving approximately the anterior two-thirds of the upper sacrum.

Pearls and Pitfalls

1. FDG is not generally used for the detection of primary bladder cancer since the tracer is excreted through urine. However, distant metastatic disease is usually seen.
2. 11C-choline and 11C-acetate have potential for bladder tumor imaging because they are not excreted in the urine [3].
3. PET has sensitivity of 67 %, specificity of 86 %, and an accuracy of 80 % for staging bladder cancer [4–6].

Discussion

Most cases of bladder cancer are transitional cell carcinoma. It is more common in whites than blacks. The median age is 68 years. Smoking, industrial carcinogen exposure, and prior radiation are risk factors. Microscopic hematuria is a common finding. IVP can be used to image the upper-tract urothelium in patients presenting with hematuria. CT and ultrasonography can be effective for lesion detection, but they can miss urothelial tumors in the upper tract. Cystoscopy and urine cytology are diagnostic. More than 70 % of the cancers are carcinoma in situ. Intravesical immunotherapy and intravesical chemotherapy are common treatment modalities. The methotrexate, vinblastine, Adriamycin, and cisplatin combination is the standard treatment for metastatic bladder cancer. For superficial bladder cancer, the 5-year survival is 82–100 %. For T2, T3, and T4 tumors, the 5-year survival rates are 63–83 %, 45–55 %, and 0–22 %. Recognition of epidural disease should prompt urgent consultation to initiate local therapy (radiation or surgery) if there is compromise of the spinal cord on MRI.

Renal Cell Carcinoma

Case 8.9

History

An 85-year-old female with history of right renal cell carcinoma, status post right radical nephrectomy. Patient developed metastasis to the left lung 11 years later for which she underwent left wedge resection with mediastinal lymphadenectomy. PET-CT is done as part of the subsequent treatment strategy evaluation.

Findings

Status post interval resection of hypermetabolic metastatic mass in the left upper lobe with postsurgical changes in comparison to baseline PET-CT (Fig. 8.9). There is increased confluence of airspace disease/bronchiectatic changes seen in the inferior right middle lobe which has increased in metabolic activity, currently demonstrating SUVmax 13.4 (previously 7.1). Again noted, patient is status post right nephrectomy with right adrenalectomy.

Impression

Status post interval resection of hypermetabolic metastatic mass in the left upper lobe. Bronchiectatic changes are seen in the right middle lobe which demonstrates increased metabolic activity, most probably inflammatory.

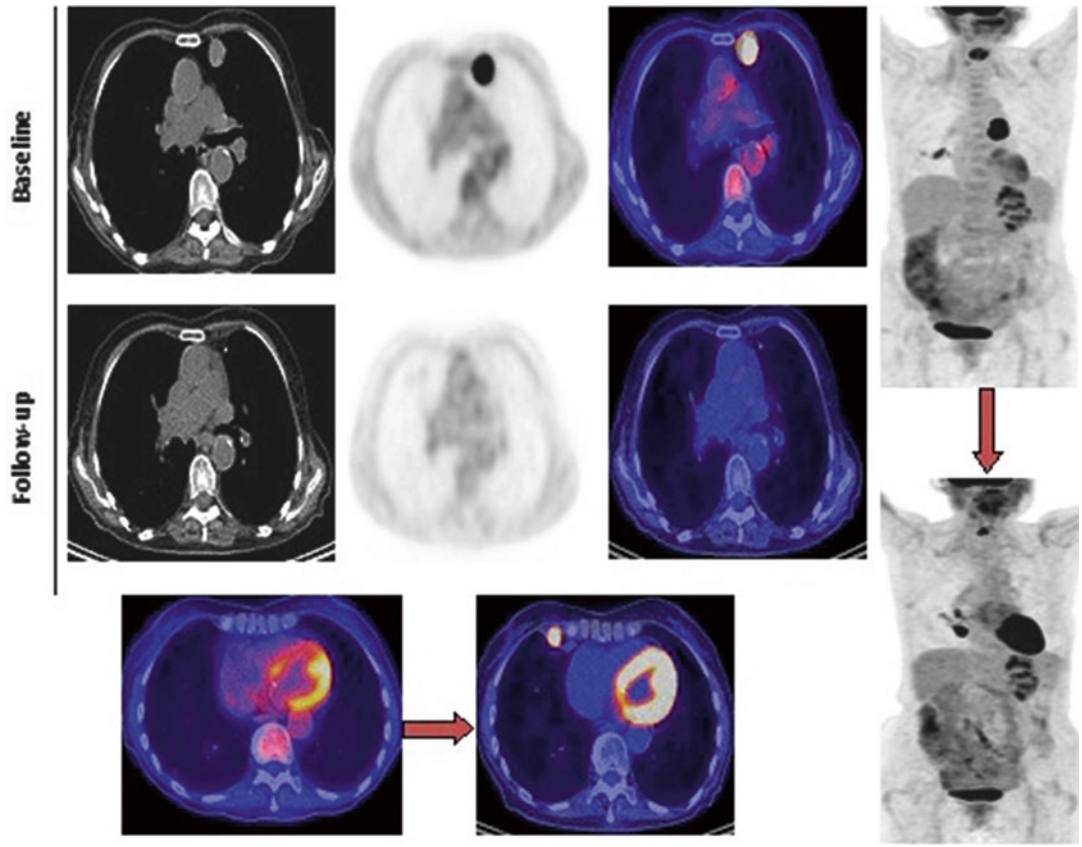

Fig. 8.9

Case 8.10

History

A 90-year-old male with high-grade transitional renal cell carcinoma and recurrent hematuria, status post resection of right renal lower pole. Pathology report showed high-grade papillary urothelial carcinoma, grade 4/4. PET-CT was done for staging purposes.

Findings

Within the right low pelvicalyceal system, in the expected area of filling defect on the CT, there is focal hyperactivity (SUVmax 7.7) (Fig. 8.10). Central calyx of the right kidney showed SUVmax 5.0, probably related to the urine. The close proximity to the urine makes it somewhat difficult to differentiate; however, the area of activity related to filling defect is suspicious for recurrent carcinoma. There is an exophytic renal cyst in the right upper pole and an intra-cortical cyst in the lower pole.

Impression

Suspect hypermetabolic recurrent malignancy within the low right renal pelvicalyceal system.

Pearls and Pitfalls

1. Seventy-seven percent of the renal cell carcinomas may be identified correctly with PET [7, 8].
2. Both PET and CT perform well in detecting metastatic lesions, 80 % as opposed to 83 %, respectively [7, 8].
3. The sensitivity, specificity, and diagnostic accuracy of PET is 82 %, 88 %, and 84 %, respectively [7, 8].
4. PET can alter patient management in 40 % of the cases [7, 8].

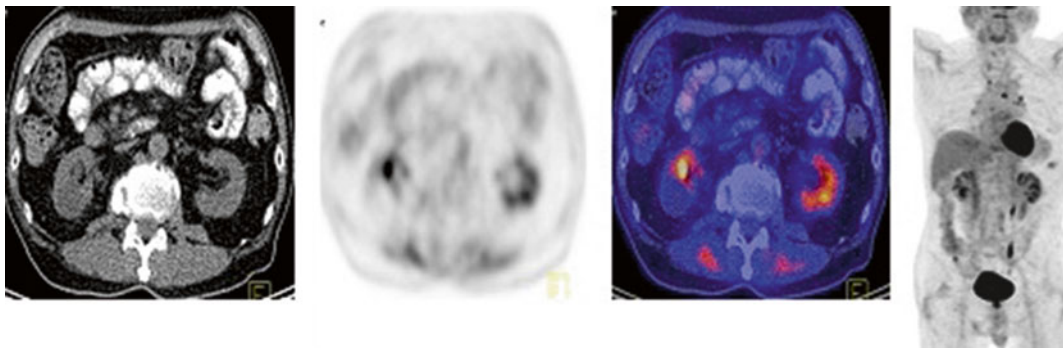

Fig. 8.10

Discussion

Renal cell carcinoma represents 3 % of all cancers in the adult population; mostly within the age range of 50–70 years of age. The widespread use of conventional CT, MRI, and ultrasonography of the abdomen has resulted in the identification of an increased number of incidental renal abnormalities, which may need further investigation. CT scanning is currently the commonly used noninvasive imaging tool to assess the nature of these abnormalities. In a study involving 53 patients, the accuracy of this technique in identifying renal masses was 83 % [9, 10]. Other larger studies showed the sensitivity and specificity of CT were both over 90 % [9, 10, 17]. CT and MRI also provide important information on size, tumor extension, and vascular invasion, factors which are essential for staging patients, prognosis, and planning of surgery.

Metastatic renal cell carcinoma has a median survival of 10 months despite of nephrectomy. A shortcoming regarding FDG PET is that its success is highly dependent on tumor histology type and tumor grade [16].

References

1. SEER: The Surveillance, Epidemiology, and End Results Program (http://seer.cancer.gov)-based within the Surveillance Research Program (SRP) at the National Cancer Institute (NCI).
2. Even-Sapir E, et al. The detection of bone metastases in patients with high-risk prostate cancer: 99mTc-MDP planar bone scintigraphy, single- and multi-field-of-view SPECT, 18F-fluoride PET, and 18F-fluoride PET/CT. J Nucl Med. 2006;47:287.
3. Heicappell R, et al. Staging of pelvic lymph nodes in neoplasms of the bladder and prostate by positron emission tomography with 18F FDG. Eur Urol. 1999;36:582–7.
4. Ahlstrom H, et al. Positron emission tomography in the diagnosis and staging of urinary bladder cancer. Acta Radiol. 1996;37:180–5.
5. Bachor R, et al. Lymph node staging of bladder neck carcinoma with positron emission tomography. Urologe. 1999;38:46–50.
6. Mantzarides M, Papathanassiou D, Bonardel G, et al. High-grade lymphoma of the bladder visualized on PET. Clin Nucl Med. 2005;30:478–80.
7. Shvarts O, et al. Positron emission tomography in urologic oncology. Cancer Control. 2002;9:335–42.
8. Steffens MG, et al. Clinical role of F-18 fluorodeoxyglucose positron emission tomography for detection and management of renal cell carcinoma. J Urol. 2002;168:2127–8.
9. Powles T, Murray I, Brock C, et al. Molecular positron emission tomography and PET/CT imaging in urological malignancies. Eur Urol. 2007;51(6):1511–20.
10. Aide N, et al. Efficiency of [(18)F]FDG PET in characterizing renal cancer and detecting distant metastases: a comparison with CT. Eur J Nucl Med Mol Imaging. 2003;30:1236–45.
11. Oyama N, et al. FDG PET for evaluating the change of glucose metabolism in prostate cancer after androgen ablation. Nucl Med Commun. 2001;22:963.
12. Beheshti M, et al. Detection of bone metastases in patients with prostate cancer by 18F fluorocholine and 18F fluoride PET-CT: a comparative study. Eur J Nucl Med Mol Imaging. 2008;35:1766.

13. Jadvar H. Molecular imaging of prostate cancer with [F-18]-fluorodeoxyglucose PET. Nat Rev Urol. 2009;6:317–23.
14. Hamaoka T, et al. Tumor response interpretation with new tumor response criteria vs. the World Health Organization criteria in patients with bone-only metastatic breast cancer. Br J Cancer. 2010;102:651–7.
15. Jadvar H. Prostate cancer: PET with 18F-FDG, 18F- or 11C-acetate, and 18F- or 11C-choline. J Nucl Med. 2011;52:81–9.
16. Subhas N, Patel PV, Pannu HK, et al. Imaging of pelvic malignancies with in-line FDG PET-CT: case examples and common pitfalls of FDG PET. Radiographics. 2005;25:1031–43.
17. Kang DE, et al. Clinical use of fluorodeoxyglucose F 18 positron emission tomography for detection of renal cell carcinoma. J Urol. 2004;171:1806–69.